Rock Mechanics
and Rock Engineering 18, 77—105 (1985)

**Rock Mechanics
and Rock Engineering**

Reconnaissance of Fractured Media with Several Systems of Fractures by Means of Harmonic Techniques

By

B. Crosnier, G. Fras, and P. Jouanna

Laboratoire de Génie Civil, Montpellier, France

Summary

The method of interpreting hydraulic tests in a harmonic state described by Fras et al. (1981), is applied to a physical laboratory model which simulates a fractured rock environment with several sets of cracks of different thicknesses. Particular attention is paid to the problem of practical identification of the fracture parameters using a theoretical file of spectral signatures. These results enable to envisage an in situ survey phase using a harmonic probe that is currently being calibrated in the laboratory.

Introduction

Of the range of methods used for the reconnaissance of fractured rock media, continuous and transient hydraulic appear to be necessary for the assessment of hydraulic and geometrical characteristics. Transient tests have been developed above all for fractured oil reservoirs (Gringarten, 1971; Gringarten and Witherspoon, 1972; Wang et al., 1978), and their advantages are that they can include compressibility and/or inertia, thus providing richer information than continuous tests. However, these tests come up essentially against the possibility of setting up highly dynamic states because of the inertia of the excitation systems. A reconnaissance technique with an established dynamic state was developed by Crosnier et al. (1979), to improve on the possibilities of continuous tests without the disadvantages of classic transient tests. A sinusoiadl flow is created in this method and the resulting pressure is measured; interpretation is carried out in frequency space (Fras, 1979; Portalès, 1981), offering entirely new possibilities as compared to all known tests.

1. Description of the Method

1.1 Principle

The two-phase (matrix + water) fractured horizon fitted with a test device and boundary conditions forms a system which receives an input signal, flow $Q(t)$, and returns an output signal, the difference in head $\Delta H(t)$ at

the shaft. If the system can be considered as linear and invariable around the point of operation, input and output are linked by a convolution integral:

$$\Delta H(t) = \int_0^t h(t-\tau) \cdot Q(\tau) \cdot d\tau. \tag{1}$$

Function $h(t)$ is the impulse response of the system, i. e. the response to a flow impulse. The calculation is carried out in Laplace transformed space, by multiplying the transformed functions; s being the Laplace variable:

$$\Delta \overline{H(s)} = \overline{H(s)} \cdot \overline{Q(s)}. \tag{2}$$

Function $\overline{H(s)}$ is referred to as a system transfer function.

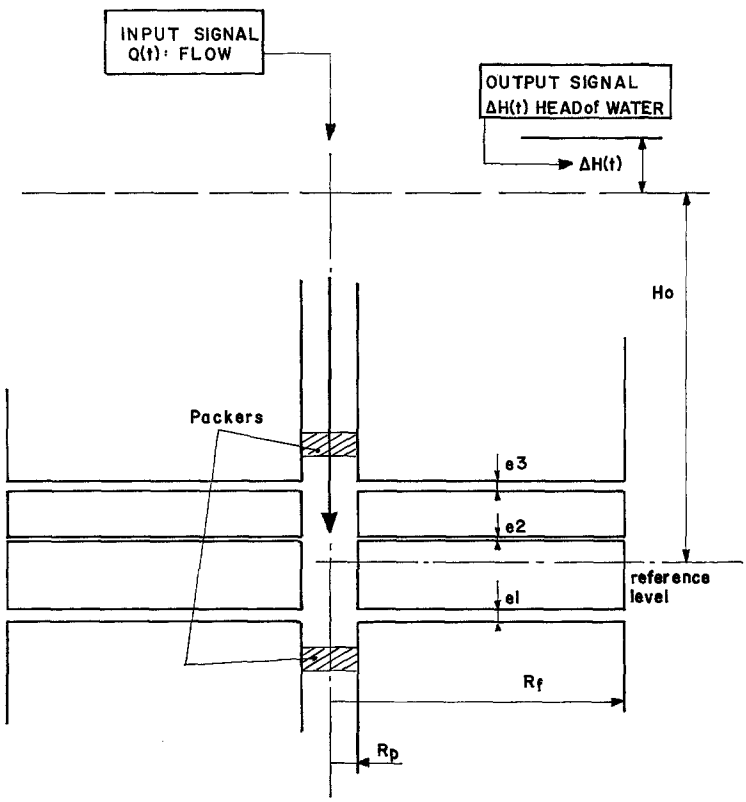

Fig. 1 a. Case studied

1.2 *Method*

Distinction can be made between three phases:

A. *Acquisition of the real transfer function of the system,* by subjecting to a signal with a sinusoidal flow at various frequencies; *harmonic pumping.*

B. *The constitution of a file of theoretical transfer functions* established from the mathematical modelling on the fractured medium studied: *direct problem.*

C. *Identification of the parameters* by comparison of the spectral signature with the transfer functions file: *inverse problem.*

1.3 Description of the Case Studied (Fig. 1a)

Fras et al. (1981) have described the experimental laboratory results concerning a system with one or two cracks of the same thickness. Here, the results of laboratory tests on systems with several groups of fractures

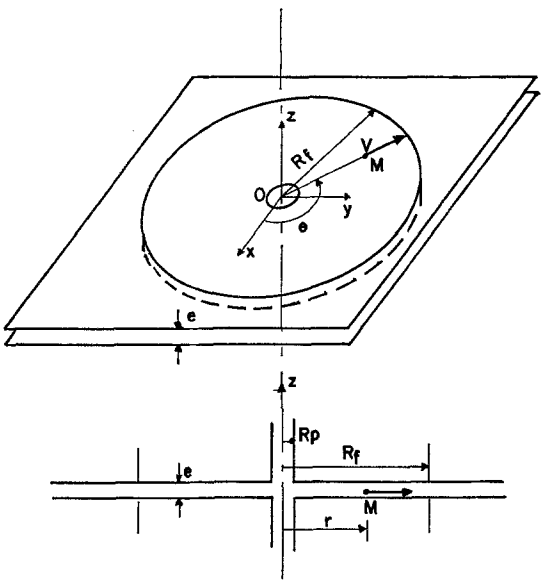

Fig. 1b. Locating a point in the fissure

of different thicknesses crossed by a boring are described. The sinusoidal flow is applied at a distance R_p from the axis of the boring, while the hydraulic head imposed is constant at a distance R_f from this axis.

2. Acquisition of the Spectral Signature

2.1 Description of the Physical Model

The experimental apparatus included:

a) the study model defining the radial flow around a boring,

b) the boundary conditions,

c) the pressure and flow measuring apparatus.

a) *The study model* (Fig. 2) consists of a duralumin plate and plexiglass plates. These plates define a flow field limited to a circular sector with an angle of 33^0 in the centre. The thickness of the various fractures thus defined can be set by means of wedges placed between the various plates and outside the flow zone. An O-ring makes the apparatus watertight and is judged to have very little effect on the flow. It is thus assumed that the radial flow conditions are fulfilled.

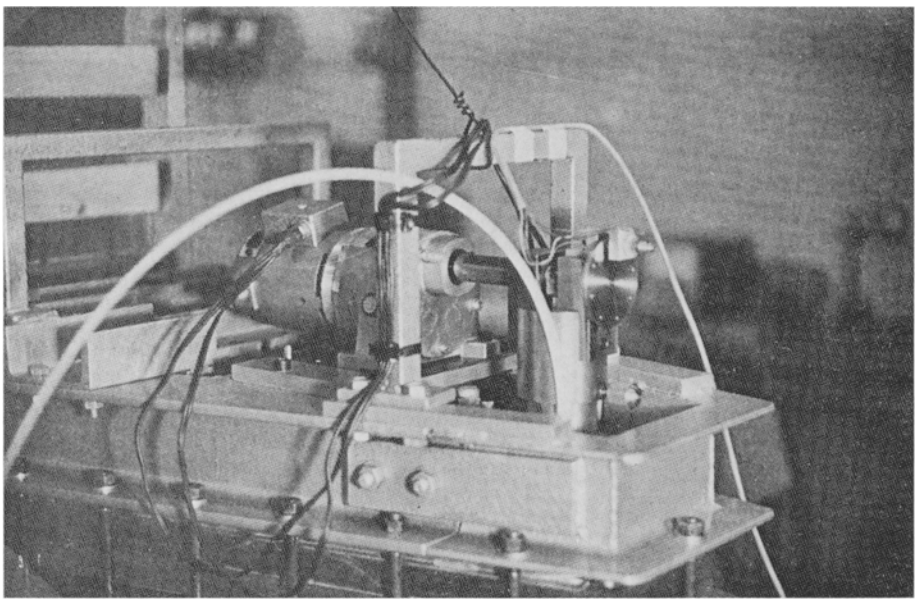

Fig. 2. Study model

b) *Boundary conditions:* Two stabilization chambers limit the flow between the plates; the internal chamber is circular, 135 mm in diameter, and represents a boring with an axis perpendicular to the fissure plane. The sinusoidal flow, generated by a piston, is set up from the chamber. The power required is provided by an electrical reduction gearing apparatus enabling motor output speeds of 6 to 700 r. p. m.; this corresponds to an explored frequency range of 0.1 Hz to 11 Hz. The external chamber, enabling the static head to be applied and maintained practically constant during the tests, is located 810 mm from the axis of the boring.

c) *Measurement apparatus* (Fig. 3): The physical quantities are the flow and the dynamic pressure set up at the entry to the fracture system. These two quantities must be measured for each excitation frequency. In general, modulus and phase of the flow and the pressure have to be measured to get the model transfer function. However, in a number of

cases, as in the present case, the determination of the modulus is sufficient for the reconnaissance of the system, as will be explained in section 4.

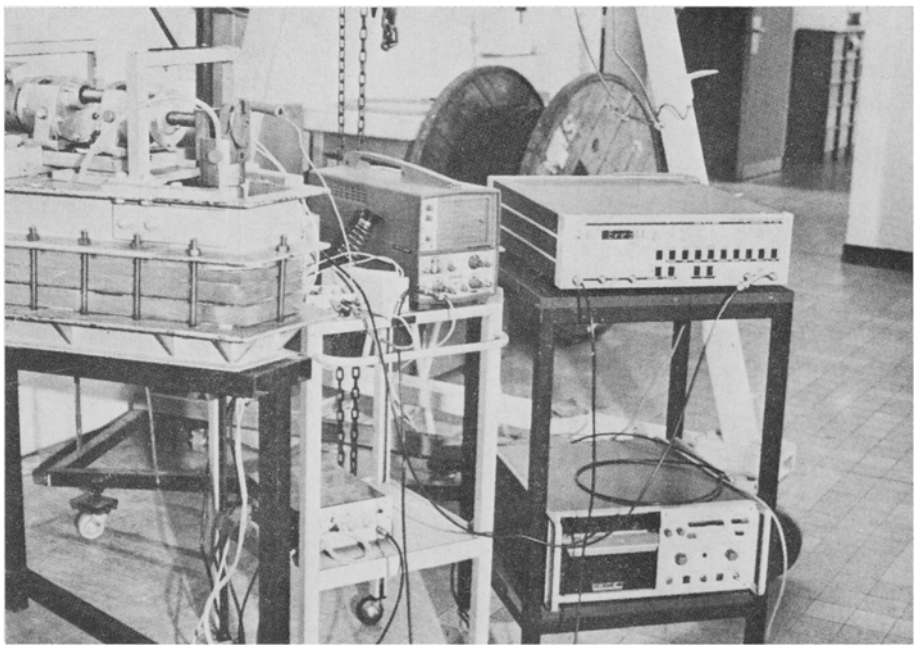

Fig. 3. Measurement apparatus

Monitoring the speed of rotation of the shaft coming out of the gearing apparatus makes it possible to calculate flow Q. This flow is, in fact, linked to the excitation frequency f and to the volume injected V during a half-stroke of the piston.

$$Q = 2\pi \cdot f \cdot \Delta V$$

where f: excitation frequency; ΔV: volume injected.

Monitoring of excitation frequency f is carried out by counting the impulses given by a photoelectric cell.

The dynamic pressure set up in the test chamber was measured by a probe with a piezoresistive membrane and with a sensitivity of 15.9 mV/cm of water. Processing of the pressure signal was carried out using a double phase synchronous detector with a minimum detectable frequency of 0.1 Hz.

Calculation of the modulus of the spectral signature was then carried out by computer.

2.2 *Harmonic Tests*

The various different experimental cases covered are given in Table 1 below.

Table 1

	Figures	Number of Sets	Total number of fractures $n=n_1+n_2$	Set (n_1, e_1)		Set (n_2, e_2)	
				n_1	e_1 (mm)	n_2	e_2 (mm)
Test 1	No. 4	1	2	2	2	0	—
Test 2	No. 5	2	2	1	2	1	1
Test 3	No. 6	2	2	1	4	1	1
Test 4	No. 7	2	3	1	4	2	1
Test 5	No. 8	2	3	1	4	2	2

2.3 Results

Only the moduli of the experimental spectral signatures obtained by the five tests are plotted in Figs. 4 to 8. These figures are represented in log-log axes as follows:

— x-axis: excitation frequency f in Hz.
— y-axis: transfer function moduli expressed in SI units, using the pressure P instead of the difference of head ΔH.

These results are discussed in paragraph 4.

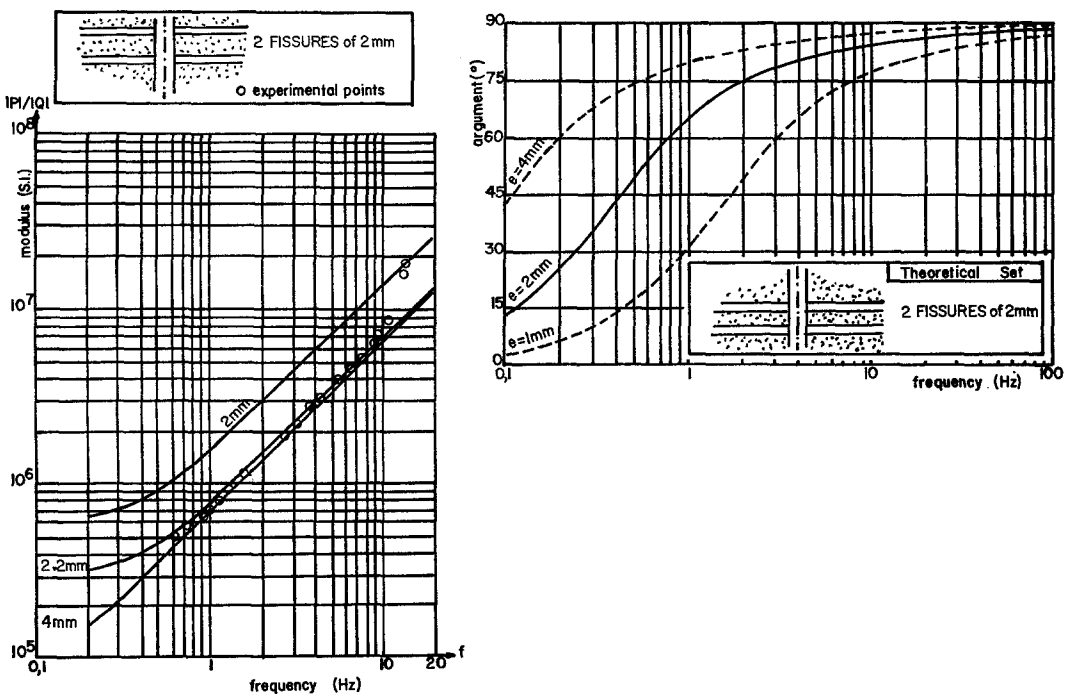

Fig. 4. Spectral signature — Test 1

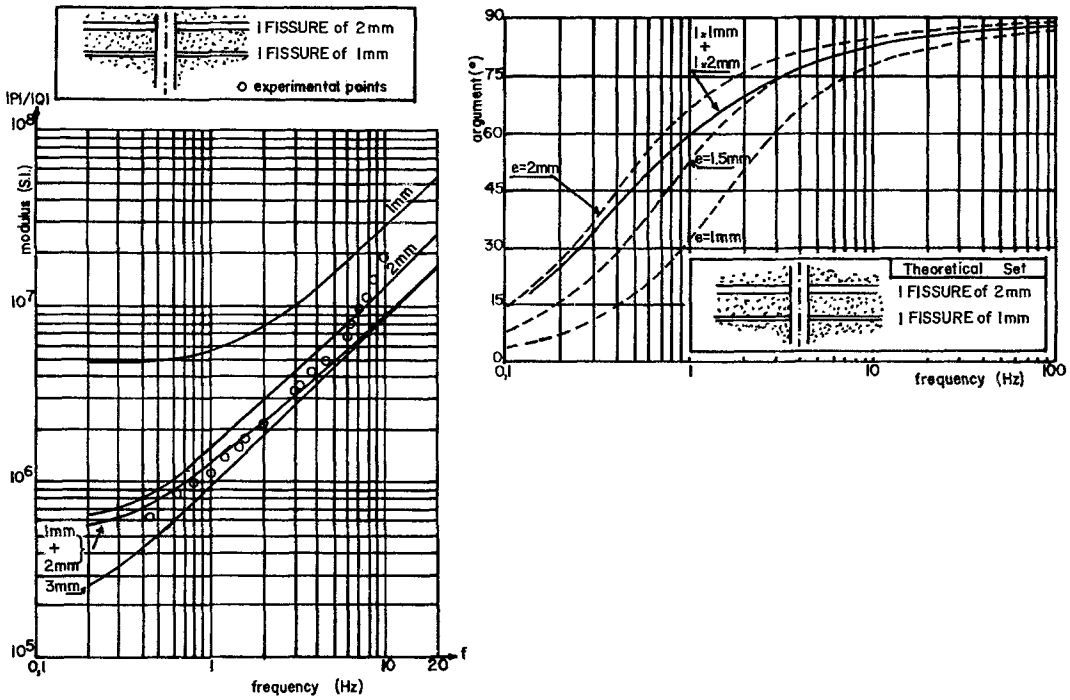

Fig. 5. Spectral signature — Test 2

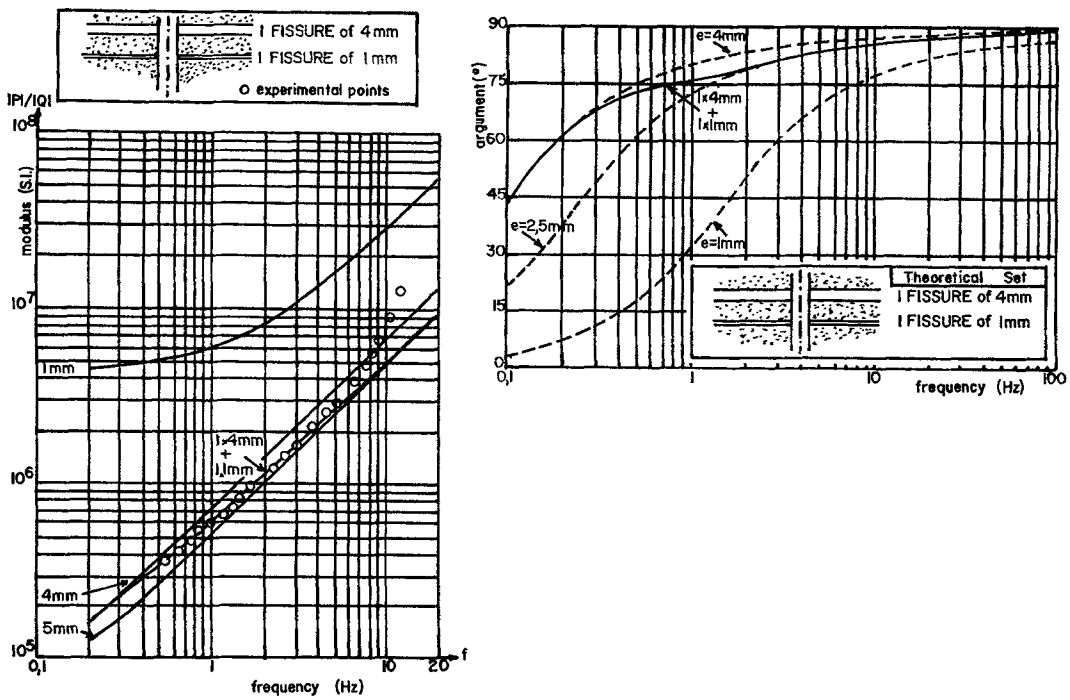

Fig. 6. Spectral signature — Test 3

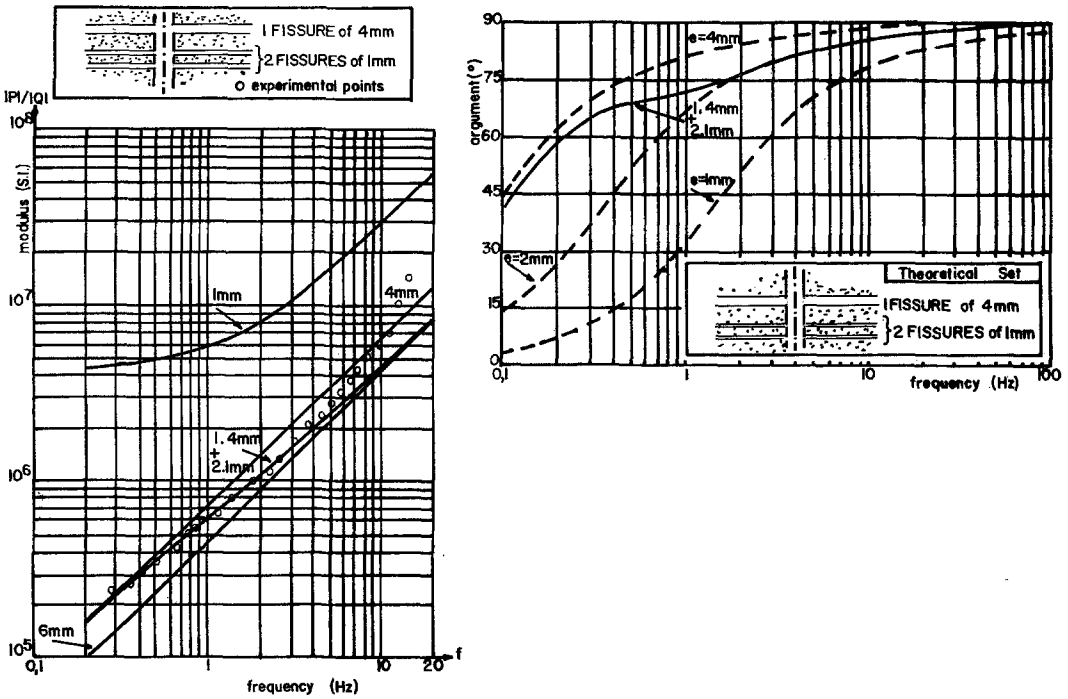

Fig. 7. Spectral signature — Test 4

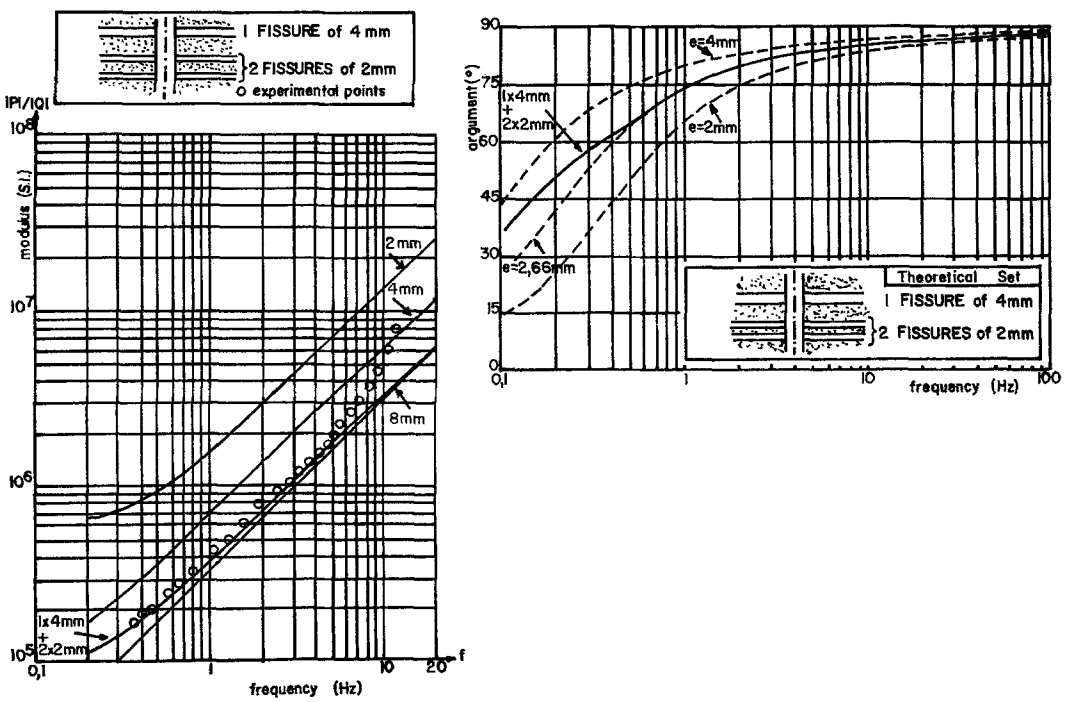

Fig. 8. Spectral signature — Test 5

3. Constitution of a File of Theoretical Transfer Functions

3.1 Schematic Representation of the Fractured Medium

The schematic representation of the experimental device is very close to the physical reality of the laboratory model and consists of a group of sets of horizontal fractures limited by a cylindrical surface with a radius R_f, coaxial to the shaft whose radius is R_p. Each set is made up of n_i fractures of the same thickness e_i (Fig. 1a). The fluid is assumed to be incompressible; its density is referred to as ϱ and its kinetic viscosity as ν. Its flow is assumed to be laminar.

In the reference state which defines the initial conditions, the head is assumed to be uniform in all the fractures, i. e. H_0. The input signal, which is the flow $Q(t)$, is assumed to run entirely into the cracks. The output signal is the difference between the instantaneous head $H(R_p, t)$ in the injection chamber and the initial head H_0. This difference is referred to as $\Delta H(t)$.

3.2 Obtaining the Transfer Functions

— *Single fracture*

a) *Flow in a fracture — equations* (Fig. 1b)

We recall the basic equations characterizing flow in a fracture developed by Fras et al. (1981).

Let a cartesian coordinate system be denoted O_{xyz}. This system is chosen in such a manner that the fissure walls are represented by two planes of equations $z=0$ and $z=e$. These walls are limited by two O_z-axis cylinders, the radius of which are respectively R_p and R_f. On the R_p-cylinder, we impose the sinusoidal flow rate, a constant charge H_0 being the condition chosen on the R_f cylinder.

We assume that the flow is radial and axis-symmetric. According to a polar coordinate system (r, θ, z) of origin, O if velocity and pressure are denoted V and P, we may deduce that these variables do not depend on θ, and tangential and vertical velocity components are zero:

$$P = P(r, z, t)$$
$$V = (U(r, z, t), 0, 0).$$

Under such conditions, if the fluid is assumed to be newtonian and incompressible, according to a local reference system (r, θ, z), the Navier-Stokes and continuity equations are to be written:

$$\frac{\partial U}{\partial t} + \frac{U \cdot \partial U}{\partial r} = -\frac{1}{\varrho}\frac{\partial P}{\partial r} + \nu\left\{\frac{\partial^2 U}{\partial r^2} + \frac{1}{r}\frac{\partial U}{\partial r} - \frac{U}{r^2} + \frac{\partial^2 U}{\partial z^2}\right\},$$

$$0 = -g - \frac{1}{\varrho}\frac{\partial P}{\partial z},$$

$$\frac{\partial (r \cdot U)}{\partial r} = 0, \quad R_p < r < R_f, \quad 0 < z < e, \quad 0 < t.$$

The second equation gives an hydrostatic distribution of the pressure along z-axis. In term of water column, pressure is given by:

$$H(r, t) = z + \frac{P(r, z, t)}{\varrho g}.$$

The initial and boundary conditions are as follows:

$$U(r, z, t=0) = 0,$$

$$H(r, t=0) = H_0,$$

$$U(r, z=0, t) = 0, \qquad U(r, z=e, t) = 0,$$

$$H(r=R_f, t) = H_0,$$

$$Q_f(t) = 2\pi R_p \cdot \int_0^e U(r=R_p, z, t)\, dz.$$

$Q_f(t)$ being the rate of flow into the fracture.

b) *Transfer function*

Solving the above system of equations, we obtain the relation (3) which expresses directly in Laplace transformed space the variation of the head $\overline{\Delta H(s)}$, in a single fracture and at its entry, in function of the flow $\overline{Q_f(s)}$ running through it, s being the Laplace variable.

$$\overline{\Delta H(s)} = \frac{\overline{Q_f(s)} \cdot s \cdot \mathrm{Log}(R_f/R_p)}{2\pi g\,[e + 2\sqrt{v/s}\,(1 - \cos h(\sqrt{s/v} \cdot e))/\sin h(\sqrt{s/v} \cdot e)]}. \tag{3}$$

— *m sets of fractures*

Attention was paid to the transfer function between the total flow $\overline{Q(s)}$ and the difference in head $\overline{\Delta H(s)}$. In this case, the total flow $\overline{Q(s)}$ is the sum of the partial flows $\overline{Q_i(s)}$ of each fracture set i:

$$\overline{Q(s)} = \sum_{i=1}^{m} \overline{Q_i(s)}.$$

In addition, it is assumed that each flow $\overline{Q_i(s)}$ is divided equally between the n_i fractures of the set of fractures under consideration. If $\overline{Q_{fi}(s)}$ refers to the flow running into a fracture of the i-th family, the following equations can be written:

$$\overline{Q_i(s)} = n_i \cdot \overline{Q_{fi}(s)}$$

$$\overline{Q(s)} = \sum_{i=1}^{m} n_i \cdot \overline{Q_{fi}(s)}. \tag{4}$$

Equation (3) can be applied to each fracture, i. e.:

$$\overline{\Delta H}(s) = \frac{\overline{Q_{fi}}(s) \cdot s \cdot \mathrm{Log}\,(R_f/R_p)}{2\pi g\, e_i \left[1 + 2\,\frac{\sqrt{v/s}}{e_i} \cdot \frac{(1-\cos h\,(\sqrt{s/v}\cdot e_i))}{\sin h\,(\sqrt{s/v}\cdot e_i)}\right]}$$

which can be written formally as follows:

$$\overline{\Delta H} = \frac{\overline{Q_{fi}} \cdot \mathrm{Log}\,(R_f/R_p)}{2\pi g \cdot e_i \cdot \bar{L}\,(e_i)} \tag{5}$$

where:

$$\bar{L}\,(e_i) = \frac{1 + 2\,\frac{\sqrt{v/s}}{e_i} \cdot \frac{(1-\cos h\,(\sqrt{s/v}\cdot e_i))}{\sin h\,(\sqrt{s/v}\cdot e_i)}}{s}.$$

If Eqs. (4) and (5) are combined, the transfer function between the total flow $\overline{Q}(s)$ and the variation in head $\overline{\Delta H}(s)$ is obtained:

$$\overline{Q}(s) = \frac{2\pi g}{\mathrm{Log}\,(R_f/R_p)} \cdot \sum_{i=1}^{m} n_i \cdot e_i \cdot \bar{L}\,(e_i) \cdot \overline{\Delta H}(s) \quad \text{and} \quad \bar{F}(s) = \frac{\Delta \bar{H}(s)}{Q(s)}.$$

The transfer function $\bar{F}$ can be represented by its modulus and its argument after replacement of s by $j\omega$, ω being the pulsation of $2\pi f$, with f being the frequency, or also by its Nyquist diagram as shown below:

a) *Modulus of the transfer function*

$$|\bar{F}| = \frac{|\Delta \bar{H}|}{|\bar{Q}|} = \frac{K\omega}{\left[\left(\sum_i n_i e_i \frac{A_i \cdot C_i + B_i}{2\beta_i (1+C_i^2)}\right)^2 + \left(\sum_i n_i e_i \left(-1 + \frac{A_i - B_i \cdot C_i}{2\beta_i (1+C_i^2)}\right)\right)^2\right]^{1/2}} \tag{6}$$

where: $K = \mathrm{Log}\,(R_f/R_p)/(2\pi g)$

$$\beta_i = \frac{e_i}{2}\sqrt{\frac{\omega}{2v}}$$

$$A_i = \mathrm{th}\,\beta_i + \mathrm{tg}\,\beta_i$$

$$B_i = \mathrm{th}\,\beta_i - \mathrm{tg}\,\beta_i$$

$$C_i = \mathrm{th}\,\beta_i \cdot \mathrm{tg}\,\beta_i$$

b) *Argument of the transfer function*

$$\mathrm{Arg}\,\bar{F} = \mathrm{Arc\,tan}\,\frac{\sum_{i=1}^{m} n_i e_i \left[1 - \frac{A_i - B_i \cdot C_i}{2\beta_i (1+C_i^2)}\right]}{\sum_{i=1}^{m} n_i e_i \left[\frac{A_i \cdot B_i + C_i}{2\beta_i (1+C_i^2)}\right]} \tag{7}$$

Formulae (6) and (7) make it possible to assemble a file of the theoretical transfer functions for m sets of fractures (n_i, e_i).

Figures 4 to 8 show the transfer functions of the various fracture systems (Table 1) studied experimentally, after replacement of the difference in head $\overline{\Delta H}(s)$ by the pressure $\overline{P}(s)$ by means of equation $\overline{P}(s) = \varrho g \overline{\Delta H}(s)$.

The values of the parameters R_p, R_f, ϱ and ν are those chosen for the physical model:

$$R_p = 6.75 \cdot 10^{-2} \text{ m} \qquad \varrho = 10^3 \text{ SI}$$
$$R_f = 8.1 \cdot 10^{-1} \text{ m} \qquad \nu = 10^{-6} \text{ SI}$$

c) *Nyquist diagram*

At a given pulsation ω, it is possible to obtain in the complex plane, a geometrical construction of vector $\overline{F}$, relative to a set of fissures, when knowing the vectors $\overline{F_1}, \overline{F_2}, \ldots \overline{F_i}, \ldots \overline{F_m}$ relative to each family of fissures.

As pressure $\overline{P}$ is assumed to be the same for all the fissures — in modulus and in phase — the total quantity of flow, i. e.:

$$\overline{Q} = \overline{Q_1} + \overline{Q_2} + \ldots + \overline{Q_i} + \ldots + \overline{Q_m}$$

becomes:

$$\frac{\overline{P}}{\overline{F}} = \frac{\overline{P}}{\overline{F_1}} + \frac{\overline{P}}{\overline{F_2}} + \ldots + \frac{\overline{P}}{\overline{F_i}} + \ldots + \frac{\overline{P}}{\overline{F_m}}.$$

The following complex relation is thus obtained relating $\overline{F}$ to the different $\overline{F_i}$:

$$\frac{1}{\overline{F}} = \sum_i \frac{1}{\overline{F_i}}. \tag{8}$$

This relation (8) allows a geometrical construction in the complex plane of $\frac{1}{\overline{F}}$, summing up the different vectors $\frac{1}{\overline{F_i}}$ (Fig. 19).

4. Identification of the Parameters

Comparison of the experimental spectral signature of a system to be surveyed and the file assembled above leads to the identification of the parameters.

The followed are examined in turn:

— the theoretical problem of the unicity of the determining of the parameters.

— analysis of the structure of the transfer function : physical and mathematical parameters.

— the practical procedure for obtaining the parameters.

— application to the case in question.

4.1 Theoretical Unicity

The transfer function appears as a function of frequency f, dependant on 2 m parameters (n_i, e_i, $i=1$ to m).

It was shown elsewhere (Portalès, 1981) that for the physical model studied in this article there is biunivocal correspondence between the set of values (n_1, e_1, n_2, e_2) and a transfer function.

In other words, a single transfer function corresponds to a fractured system made up of two fractures characterized by the values of two couples (n_i, e_i) and, reciprocally, a single set of values of these parameters corresponds to a given transfer function. Such a correspondence has also been proved in the case of 3 families of fractures.

4.2 Groups of Identifiable Parameters

Analysis of the structure of the transfer function reveals certain groupings of parameters which are identifiable by adjustment of the real spectral signature to the spectral file.

The first step is to obtain as much information as possible from the behaviour of the transfer function at low frequencies and then at high frequencies.

This behaviour is analysed below by limited expansion and asymptotic expansion of $\overline{F}$ respectively.

4.2.1 Low Frequencies

— *Modulus of* $\overline{F}$

The behaviour of $\overline{F}$ at low frequencies can be analysed using the following expression:

$$|\overline{F}| = \frac{6\,v\,\mathrm{Log}\,(R_f/R_p)}{\pi\,g} \cdot \frac{1}{\left[(\sum_i n_i e_i^3)^2 + \frac{1}{100\,v^2} \cdot (\sum_i n_i e_i^5)^2 \cdot \omega^2\right]^{1/2}} + 0\,(\omega)$$

with the following limit for ω tending towards O:

$$|\overline{F}| = \frac{6\,v\,\mathrm{Log}\,(R_f/R_p)}{\pi\,g} \cdot \frac{1}{\sum_i n_i \cdot e_i^3}. \tag{9}$$

— *Argument of* $\overline{F}$

The behaviour of Arg $\overline{F}$ at low frequencies can be analysed using:

$$\mathrm{Arg}\,\overline{F} = \mathrm{Arctan}\left[\frac{1}{10\,v} \cdot \frac{\sum_i n_i \cdot e_i^5}{\sum_i n_i \cdot e_i^3} \cdot \omega\right]. \tag{10}$$

4.2.2 High Frequencies

At high frequencies the following expressions give the modulus and the argument of the transfer function:

— *Modulus of* $\overline{F}$

$$|\overline{F}| = \frac{\text{Log}\,(R_f/R_p)}{2\pi g} \cdot \frac{\omega}{\sum_i n_i \cdot e_i}. \tag{11}$$

— *Argument of* $\overline{F}$

$$\text{Arg}\,\overline{F} = \text{Arctan}\left[\frac{\sum_i n_i \cdot e_i}{\sum_i n_i} \cdot \sqrt{\frac{\omega}{2\nu}}\right]. \tag{12}$$

4.2.3 Parameters

a) *Mathematical parameters*

The four expressions (9), (10), (11) and (12) representing the expression of the modulus and the argument of the transfer function at low and high frequencies enable the identification of 4 groups of parameters. These parameters are written as follows:

$$\begin{aligned} p_1 &= \Sigma\, n_i, & p_3 &= \Sigma\, n_i \cdot e_i^3, \\ p_2 &= \Sigma\, n_i \cdot e_i, & p_4 &= \Sigma\, n_i \cdot e_i^5. \end{aligned} \tag{13}$$

b) *Physical parameters*

The transition from the mathematical parameters (13) to the identification of the physical parameters (n_i, e_i) is carried out by inversing the formulae (13) after assigning a value to each of the parameters p_1, p_2, p_3 and p_4.

c) *Inverse problem*

If the determination of (p_1, p_2, p_3, p_4) is possible and unique, the inverse problem is said to present uniqueness as far as the mathematical parameters are concerned.

If this first step of uniqueness is verified and in order to get a complete uniqueness in the determination of the physical parameters, the inversion of formulae (13) must give one but only one solution for the set (n_i, e_i).

4.3 Example of Identification of the Mathematical and Physical Parameters

— *Assumption 1:* This example will be given assuming that only two sets of fractures (n_1, e_1) and (n_2, e_2) are present.
This is the case envisaged for the physical model given in section 2. Moreover, three different experimental possibilities will be considered:

— *Option 1:* the experimental transfer function is assumed to be entirely known on a wide range of frequencies, by its modulus and also its phase, this last measurement involving a rather sophisticated device.

— *Option 2:* the experimental transfer function is assumed to be known on a wide range of frequencies, only by its modulus, the experimental measuring device being too simple to give the phase.

— *Option 3:* the experimental transfer function is assumed to be known only by its modulus, but only in a medium range of frequencies.

4.3.1 Option 1: Identification Using the Modulus and the Phase

A) *Identification of the mathematical parameters* (p_1, p_2, p_3, p_4)

a) *Modulus of* $\bar{F}$

Low frequencies: when $\omega \to 0$, the theoretical approximation of $|\bar{F}|$ given by formula (9) shows that the modulus of the signature tends towards the horizontal.

When determining the real spectral signature, the range of low frequencies has to be wide enough to investigate this "horizontal" portion of the curve, to obtain the value of:

$$p_3 = n_1 e_1^3 + n_2 e_2^3. \tag{14a}$$

High frequencies: when $\omega \to \infty$, the theoretical approximation of $|\bar{F}|$, given by formula (11) shows that the modulus of the spectral signature, in log-log axis, has a slope equal to 1.

When determining the real spectral signature, the range of high frequencies has to be large enough to investigate the portion of the curve tending to this 45^0 inclination. Any particular point A $[\omega_A, |\bar{F}|_A]$ on this portion of curve leads, by formula (11), to the determination of:

$$p_2 = n_1 \cdot e_1 + n_2 e_2. \tag{14b}$$

b) *Argument of* $\bar{F}$

Low frequencies: when $\omega \to 0$, the theoretical approximation of Arg $\bar{F}$, given by formula (10), suggests plotting tan [Arg $\bar{F}$] versus ω, in log-log axis. In such a representation, the spectral signature has, when $\omega \to 0$, a slope, equal to 1.

When the real signature in the representation stated above, approaches a line inclined at 45^0, any point $[\omega_B, \tan (\text{Arg } \bar{F})_B]$ on this portion of the curve can be taken in order to compute, by formula (10), the value of the ratio p_4/p_3. As the value of p_3 is known by (14a), the value of p_4 is thus obtained:

$$p_4 = n_1 e_1^5 + n_2 e_2^5. \tag{14c}$$

High frequencies: when $\omega \to \infty$, the theoretical approximation of Arg $\bar{F}$, given by formula (12), suggests, as above, plotting tan (Arg $\bar{F}$) versus ω, in log-log axis. In such a representation, the spectral signature has, when $\omega \to \infty$, a slope equal to 1/2.

When the real signature, at high frequencies, approaches this slope, any point C [ω_C, tan (Arg F)$_C$] leads, by formula (12), to the value of the ratio p_2/p_1. Knowing the value of p_2 by (14b), the value of p_1 is thus obtained:

$$p_1 = n_1 + n_2. \tag{14d}$$

In conclusion, in the present case, the inverse problem presents uniqueness, as far as the mathematical parameters are concerned.

Moreover, in this case, the determination of (p_1, p_2, p_3, p_4) requires only the knowledge of the spectral signature at low and high frequencies, the medium range of frequencies not being theoretically necessary.

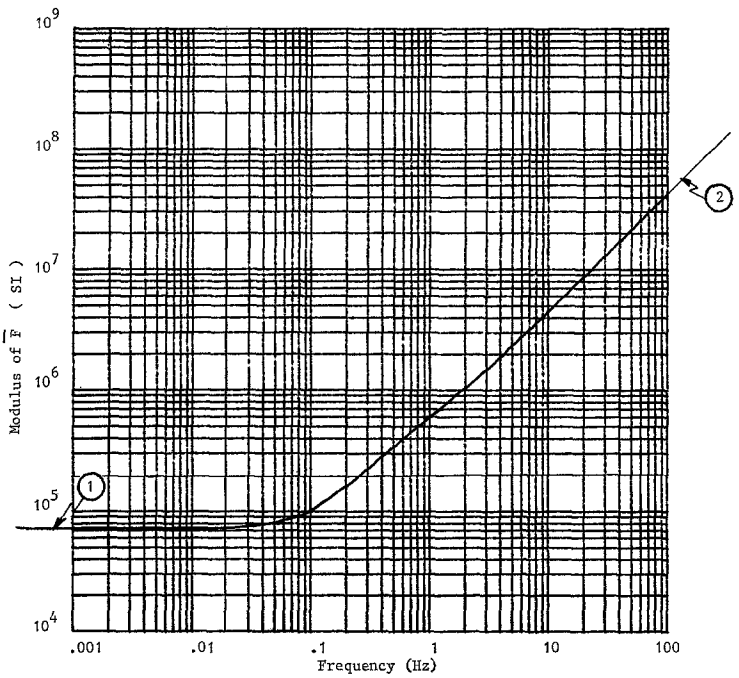

Fig. 9 a. Asymptotic behaviour of modulus
Low frequencies: (1) Slope = 0
High frequencies: (2) Slope = 1
(Example of test 4)

The summary of these results appears in Figs. 9, under the conditions of test 4 (Fig. 9a for modulus and Fig. 9b for tan (arg.)).

B) *Identification of physical parameters* (n_1, e_1, n_2, e_2)

As stated in paragraph 4.2.3, if inversion of formulae (14a to d) leads to one and only one solution (n_1, e_1, n_2, e_2), the determination of the physical parameters will be unique.

Property: It can be shown that this inversion, in the general case of two families of fractures, leads to a unique analytical solution giving (n_1, e_1, n_2, e_2) (Crosnier, 1983).

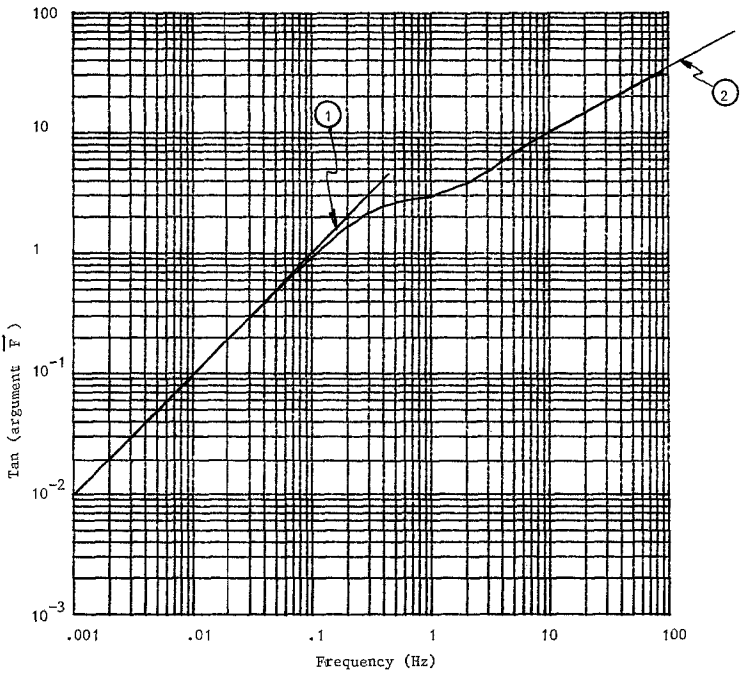

Fig. 9b. Asymptotic behaviour of tan (argument)
Low frequencies: (1) Slope = 1
High frequencies: (2) Slope = 1/2
(Example of test 4)

Simplifying assumption 2: To avoid the complexity of a general demonstration of the preceding property — complexity of no interest here — the following identification of the physical parameters will be presented using the simplifying assumption, according to which e_1 is much larger than e_2, the number of fractures n_1 and n_2 being of the same order of magnitude.

Inversion of formulae (14a to d): According to the simplifying assumption 2, relations (14a) and (14c) become:

$$p_3 \cong n_1 \cdot e_1^3$$

$$p_4 \cong n_1 \cdot e_1^5$$

from which are immediately taken the values of e_1 and n_1:

$$e_1 = \sqrt{\frac{p_4}{p_3}} \quad \text{and} \quad n_1 = \frac{(p_3)^{5/2}}{(p_4)^{3/2}}. \tag{15}$$

These values plus relations (14d) and (14b) given by:

$$\left| \begin{array}{l} p_1 = n_1 + n_2 \\ p_2 = n_1\, e_1 + n_2\, e_2 \end{array} \right. \tag{16}$$

lead to the values of e_2 and n_2:

$$\left| \begin{array}{l} e_2 = \dfrac{p_2 - (p_3)^2/p_4}{p_1 - (p_3)^{5/2}/(p_4)^{3/2}} \\ n_2 = p_1 - \dfrac{(p_3)^{5/2}}{(p_4)^{3/2}}. \end{array} \right. \tag{17}$$

C) *Illustration*

Forgetting for a while the values of the parameters (n_i, e_i) fixed on the physical model, a complete inverse problem analysis should be possible using only the recorded curves of modulus and phase in order to obtain (n_i, e_i) from these curves.

This was not done in these preliminary tests for two reasons:

— The range of frequencies was not wide enough, towards low frequencies.

— The phase curve was not recorded.

In consequence only an illustration of the theoretical results compared to the experimental results is given here with the help of the parameter values (n_i, e_i), which are assumed to be known.

Theoretical and experimental results are discussed for test 4, reported in Fig. 7, for which the simplifying assumption 2 is well satisfied as shown below.

For	$n_1 = 1$	$e_1 = 4$ mm
and	$n_2 = 2$	$e_2 = 1$ mm.

Exact and approximate values of p_3 amd p_4 are the following:

Exact values	$p_3 = 6.6 \cdot 10^{-8}$	$p_4 = 1.026 \cdot 10^{-12}$
Approximate values	$\tilde{p}_3 = 6.4 \cdot 10^{-8}$	$\tilde{p}_4 = 1.024 \cdot 10^{-12}$.

In such a case the following observations can be made (Fig. 7):

a) *Modulus* $|\overline{F}|$

At *low frequencies* the modulus curve behaves as if only the larger fissures were present (1 fissure of 4 mm).

At *high frequencies,* the modulus curve behaves as for only one fissure of thickness $\Sigma\, n_i\, e_i$, that is the cumulative thickness of the whole system (1 fissure of 6 mm). Some limitations in high frequencies are examined in paragraph 5.2.

b) *Phase of Arg* $|\bar{F}|$

At *low frequencies*, the phase curve behaves as if only the larger fissures were present (1 fissure of 4 mm).

At *high frequencies*, the phase curve behaves as for only one fissure, its thickness being equal to the barycentric value: $\Sigma\, n_i e_i / \Sigma\, n_i$ (1 fissure of 2.0 mm).

Such observations can be made on other tests, with a more or less good agreement depending on the validity of simplifying assumption 2.

However is must be stressed again that this assumption has been used here only for ease of discussion.

4.3.2 Option 2 — Identification Using the Modulus Alone

A) *Identification of the mathematical parameter (p_3 and p_2) by modulus of $\bar{F}$ only*

As described above, only two mathematical parameters, p_3 and p_2, can be obtained with knowledge of modulus $|\bar{F}|$ at low and high frequencies:

$$p_3 = n_1\, e_1{}^3 + n_2\, e_2{}^3, \tag{14b}$$

$$p_2 = n_1\, e_1 \; + n_2\, e_2. \tag{14c}$$

B) *Identification of the physical parameters*

Of course in the general case of 2 sets of fissure it is no longer possible to obtain (n_1, e_1, n_2, e_2) from p_3 and p_2. However under the simplifying assumption 2, as stated above, a determination of (n_1, e_1, n_2, e_2) is nevertheless possible as shown below.

Low frequencies: Using assumption 2, we obtain:

$$p_3 \cong n_1\, e_1{}^3. \tag{14b'}$$

This value of p_3 defines a group of curves with the same $n_1\, e_1{}^3$ at low frequencies, when the effect of (n_2, e_2) is neglected. These curves for $n_1 = 1$; $n_1 = 2, \ldots,$ and the corresponding values of e_1, can be drawn using Eq. (6), as shown in Fig. 10a. Around $\omega = 0$, the comparison of the shape of the real spectral signature with this file of curves, leads to the value of n_1.

Thus the parameter (n_1, e_1) with assumption 2, are still obtained, using not only the asymptotic value of $|\bar{F}|$, when $\omega \to 0$, but also the shape of the spectral signature in the vicinity of $\omega = 0$.

High frequencies: The asymptotic behaviour, as indicated above, leads to the value of:

$$p_2 = n_1\, e_1 + n_2\, e_2.$$

As (n_1, e_1) is known as shown above, the group $n_2\, e_2$ is thus obtained.

Knowing now n_1, e_1 and the product $n_2\, e_2$ it is possible to draw at high frequencies, using (6), a group of curves for values $n_2 = 1$, $n_2 = 2$, etc.

and the corresponding values of e_2, for the known value of the product $n_2\, e_2$, as shown in Fig. 10b.

The shape of the true spectral signature is compared to the set of curves defined by n_1, e_1 and $n_2\, e_2$ — leading to the value n_2 and therefore e_2.

Conclusion: Thus knowing (n_1, e_1) from the shape of the real spectral signature in the vicinity of $\omega = 0$, and knowing (n_2, e_2) from the shape of the real spectral signature in the vicinity of $\omega \to \infty$, the values (n_1, e_1, n_2, e_2) are obtained analyzing only the modulus of $\overline{F}$.

C) *Illustration*

In Fig. 10a and b an illustration of the whole process of determination of (n_1, e_1, n_2, e_2) is given using the modulus $|\overline{F}(\omega)|$ alone.

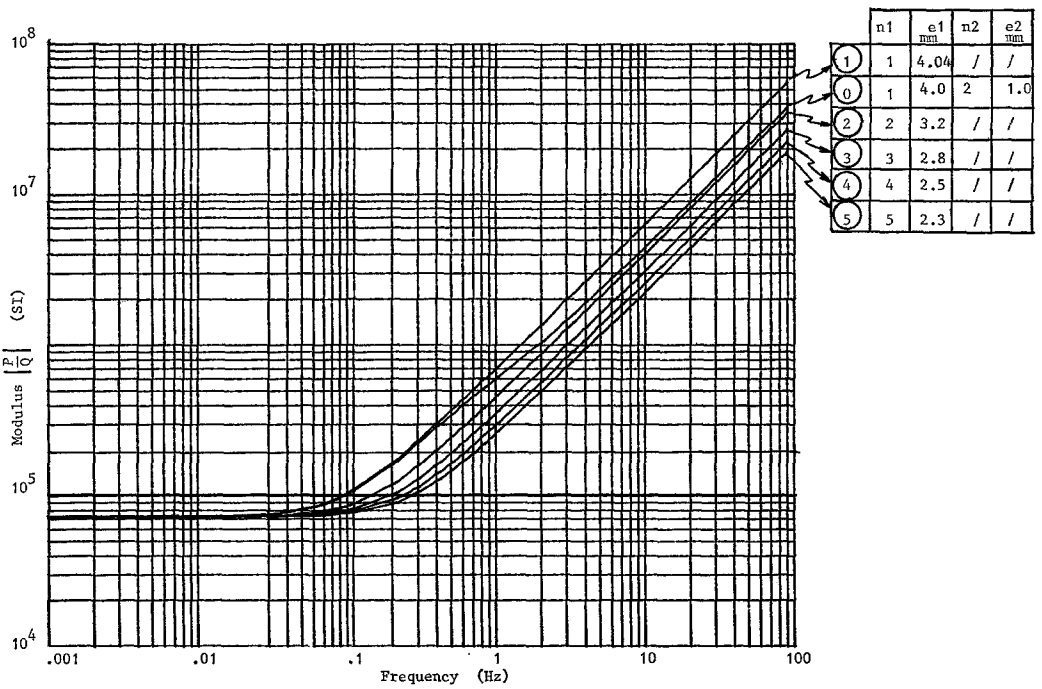

Fig. 10 a. Identification using modulus at low frequencies
Low frequencies: $\Sigma\, n_i e_i^3 = 66 \cdot 10^{-9}$ SI

As an application the case of the system used in the laboratory for test 4 could still be used. However the recording of the experimental spectral signature being made only in the medium range of frequencies, this example gives only an illustration of the determination of (n_1, e_1, n_2, e_2), a case satisfying assumption 2 but ignoring the phase curve. From Fig. 10a, the value $n_1 = 1$ is obtained leading to $e_1 \cong 4.04$ mm. From Fig. 10b, the value of $n_2 = 2$ is obtained leading to $e_2 \cong 1$ mm but with some difficulties, the different curves being close to each other.

4.3.3 Option 3 — Identification Using the Modulus Alone in a Medium Range of Frequencies

In some cases, the knowledge of the modulus of the spectral signature can be limited only to medium frequencies. This fact can be due to the inability of the measuring device, to obtain results at very low frequencies. At high frequencies, the excitation device can impose some limitation due to appearance of turbulence phenomena, as explained in section 5.

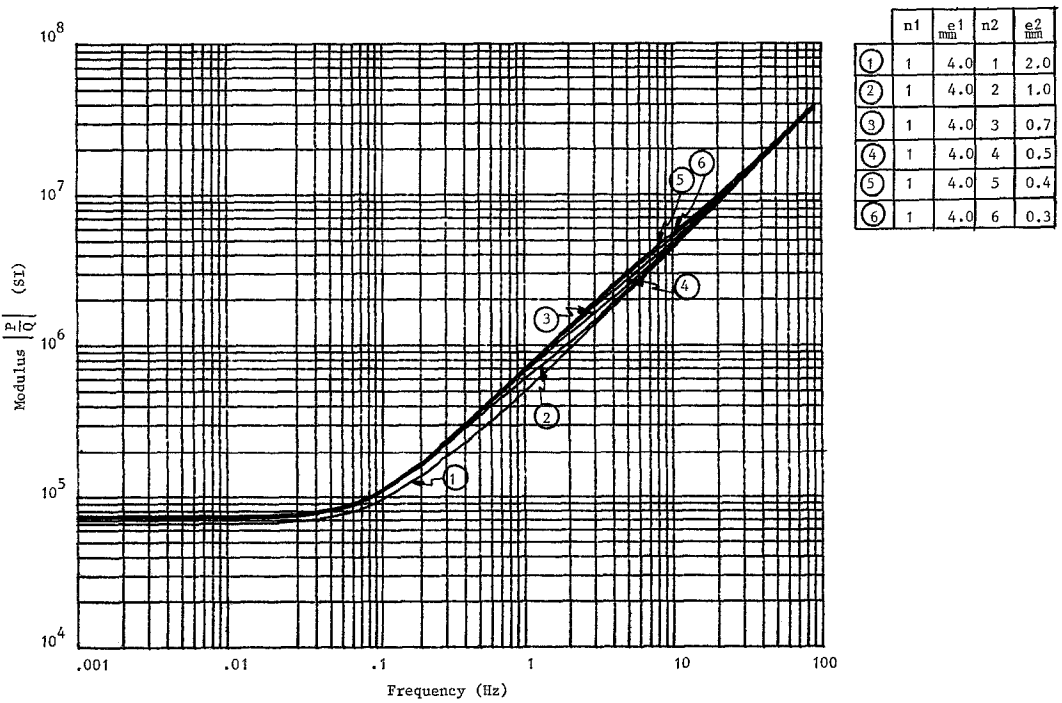

	n1	e1 mm	n2	e2 mm
1	1	4.0	1	2.0
2	1	4.0	2	1.0
3	1	4.0	3	0.7
4	1	4.0	4	0.5
5	1	4.0	5	0.4
6	1	4.0	6	0.3

Fig. 10b. Identification using modulus at high frequencies
High frequencies: $\Sigma n_i e_i = 6 \cdot 10^{-3}$ SI

— *Method:* In such a case, the method consists in taking into account the whole shape of the spectral signature, the informations given by the asymptotic behaviour of this signature being no longer available in low or high frequency domains.

— *Illustration*

A) *1st step*

The experimental curve, drawn as above in log-log axis, is compared to a file of spectral signatures established for one family of fissures of thickness e and for different numbers of fissures.

For example Fig. 11 shows the spectral signature given by Eq. (6) for a thickness $e = 10^{-3}$ m and for n varying between 1 and 10.

Figs. 11 to 17 give different files established for families of thickness $e=10^{-3}$ m to $e=8\cdot10^{-3}$ m.

As an illustration the experimental signature obtained in test No. 4 [$n_1=1$; $e_1=4$ mm; $n_2=2$; $e_2=1$ mm] is compared to these different files.

— *1st operation: matching towards low frequencies:* The shape of the real curve fits, at low frequencies, the theoretical curve of file Fig. 14, giving $n_1=1$ and $e_1=4$ mm, assuming that the thinner fissures do not influence results at low frequencies.

— *2nd operation: matching, towards high frequencies:* The shape of the real curve fits, at higher frequencies, the curve for one family of thickness $\Sigma n_i e_i$.

For example the real curve should fit curve $n=1$ of Fig. 16, corresponding to one fissure of thickness 6 mm. (This is not exactly the case, due to

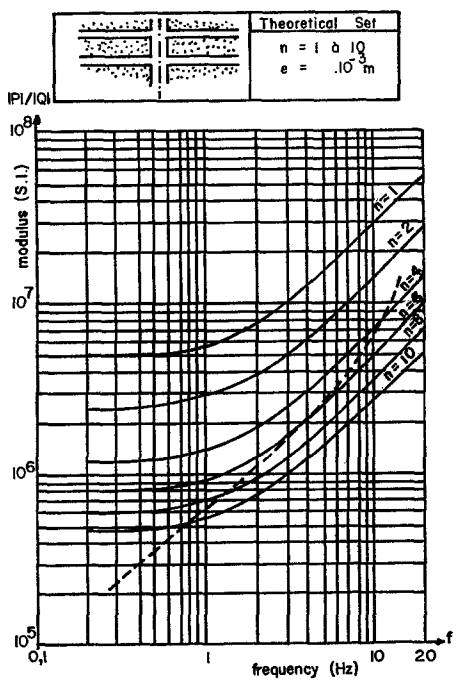

Fig. 11

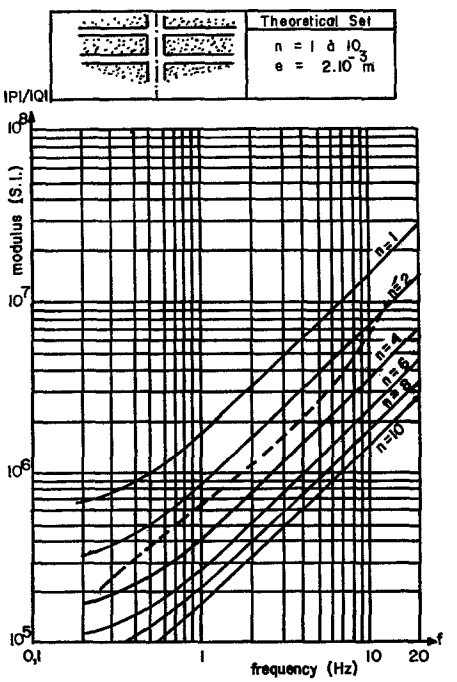

Fig. 12

Fig. 11. File of transfer functions ($n=1$ to 10; $e=$ 10^{-3})

Fig. 12. File of transfer functions ($n=1$ to 10; $e=2\cdot10^{-3}$)

Fig. 13. File of transfer functions ($n=1$ to 10; $e=3\cdot10^{-3}$)

Fig. 14. File of transfer functions ($n=1$ to 10; $e=4\cdot10^{-3}$)

Fig. 15. File of transfer functions ($n=1$ to 10; $e=5\cdot10^{-3}$)

Fig. 16. File of transfer functions ($n=1$ to 10; $e=6\cdot10^{-3}$)

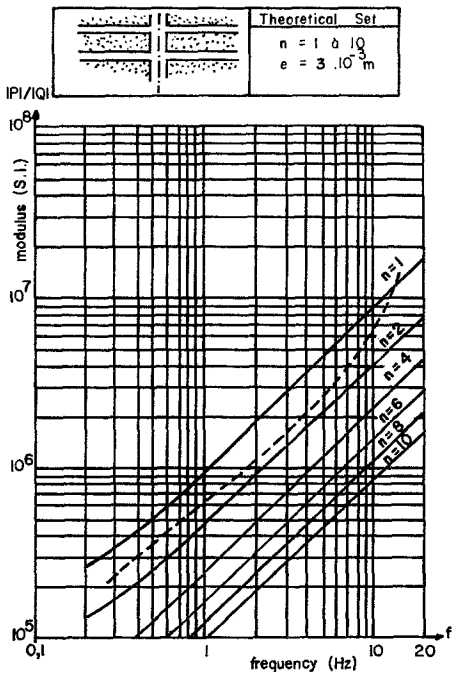

Fig. 13

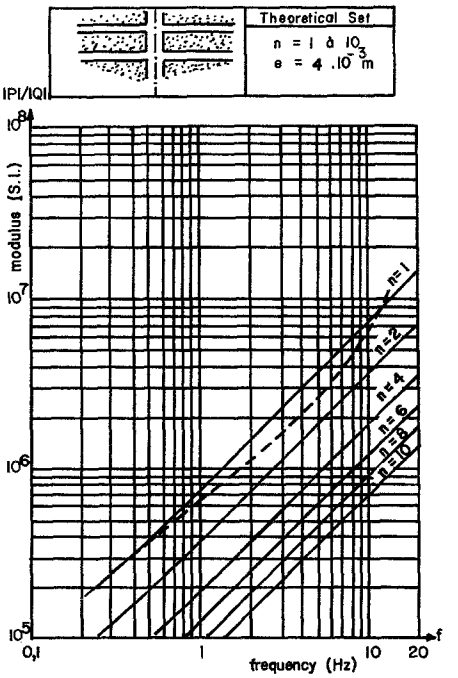

Fig. 14

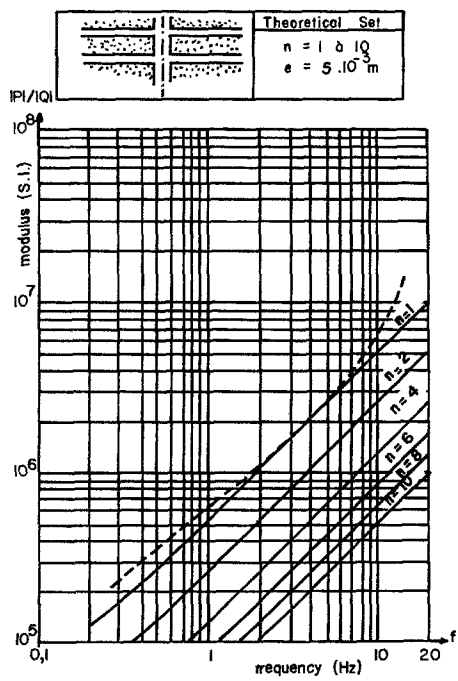

Fig. 15

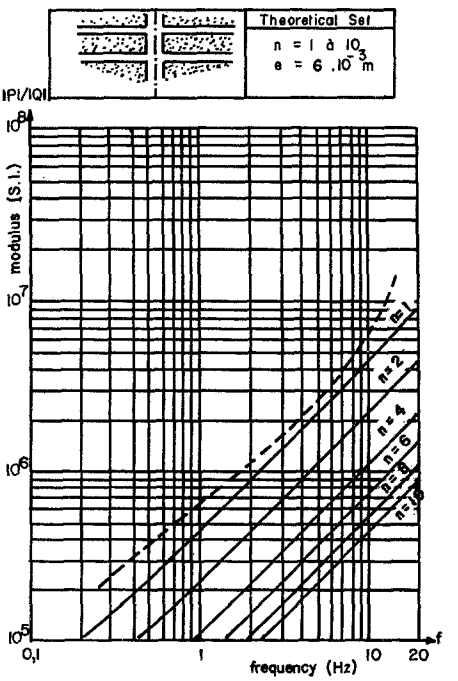

Fig. 16

turbulence effects, as explained in section 5, the volume of the piston being too large here).

Thus $n_1 e_1 + n_2 e_2 = 6$ mm, and ($n_1 = 1$; $e_1 = 4$ mm) give the value of $n_2 e_2 = 2 \cdot 10^{-3}$ SI.

B) *2nd step*

Knowing the previous information it is now possible to plot a file of theoretical signatures, using Eq. (6), for a given set ($n_1 e_1$, n_2, e_2,) taking as a parameter n_2.

The matching of this file and the experimental curve leads to the value of n_2 and consequently to the value of e_2.

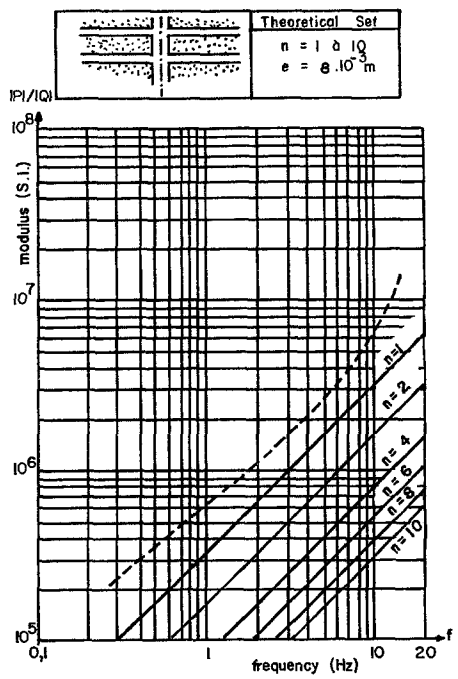

Fig. 17

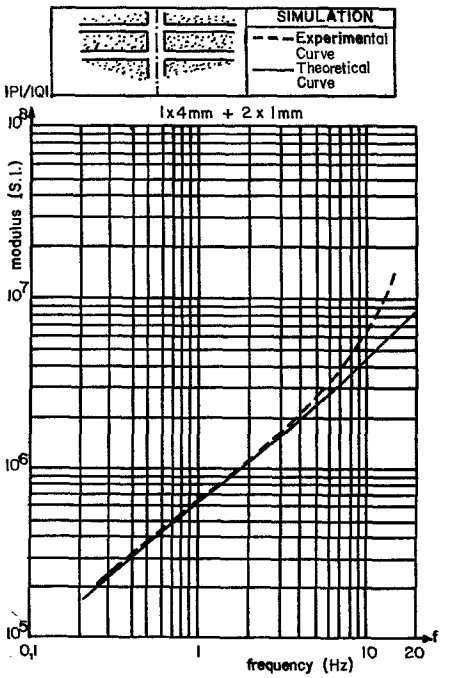

Fig. 18

Fig. 17. File of transfer functions ($n = 1$ to 10; $e = 8 \cdot 10^{-3}$)

Fig. 18. Matching between experimental and theoretical curve

Thus for the example of test No. 4, Fig. 18 gives the final matching of the experimental curve and the theoretical curve for ($n_1 = 1$; $e_1 = 4$ mm; $n_2 = 2$, $e_2 = 1$ mm).

4.3.4 Comparison Between Option 1, Option 2 and Option 3

The identification of parameters by option 1 using the modulus and the phase of the transfer function, on a large frequency bandwidth, gives of course the best results.

The use of the shape of the curves in low and high frequencies in option 2 — or the use of the shape of the total spectral signature in option 3 — should in fact appear as a confirmation of the value of the parameters, as given by option 1 and also a confirmation of the value of the type of model used.

5. Discussion of the Method in the Case of Inertia-Viscosity Models

Passing from theory to practice, three main questions arise:

a) What is the influence of the theoretical model chosen for elaborating the inverse problem?
b) For a given model, what is the sensitivity of the parameter identification?
c) What are the limitations imposed by the linear assumption, necessary for all treatment by Fourier transform?

Points b and c are discussed below. A class of inertia-viscosity models is assumed, this class fitting the experimental device adopted for the present qualification of the harmonic method in the case of several fracture families.

5.1 Resolution Capacity of the Method

— *Direct problem:* Perfect superimposition of the curve of the theoretical modulus and the experimental points is observed in the five tests; this is the case for the medium range of frequencies up to 6 Hz (Figs. 4 to 8).

— *Inverse problem:* An idea of the sensitivity of the inverse problem can be approached by examining Figs. 10a and 10b.

It appears that reducing the number n_1 or n_2 of the fractures to be examined leads to better separation of the file curves and thus enables better matching with the real spectral signature.

Practically speaking, this means that the zone to be investigated in a well should be as limited as possible.

Of course this sensitivity should be much affected if the frequency bandwidth were narrow. To get a wide bandwidth depends on the recording instrumentation but depends also, at high frequencies, on the excitation system, as explained below.

5.2 Linear Behaviour Limitations at High Frequencies

Examination of the experimental results obtained for the 5 tests carried out shows that the lack of correspondence between the theoretical and experimental curves is located higher than a critical frequency f_c, located at around 5 Hz.

This critical frequency f_c corresponds, as shown below, to a change from laminar flow to turbulent flow, obtained when the Reynolds Number $R_e = \frac{V \cdot 2e}{\nu}$ exceeds a critical value of 2300, V being the velocity in the fissure of thickness e.

The expression of R_e indicates that the critical Reynolds Number will appear first in the thicker fissures. For example in test No. 4, turbulence will appear in the one fissure of thickness $e_1 = 4$ mm, while flow will remain laminar in the two fissures of thickness $e_2 = 1$ mm.

In this case of test No. 4, the following assumptions can be made to approach the value of f_c:

a) *Assumption 1:* The velocities V_1 in fissures e_1, and velocities V_2 in the thinner fissures, are in phase (see foot-note[1]). Thus:

$$|\overline{Q}(f)| = |\overline{Q_i(f)}| + |\overline{Q_2(f)}|.$$

b) *Assumption 2:* Laminar flow in radial fissures, at low frequencies, is assumed to be proportional to $n e^3$. Thus:

$$\frac{|\overline{Q_1(f)}|}{n_1 e_1^3} = \frac{|\overline{Q_2(f)}|}{n_2 e_2^3} = \frac{|\overline{Q_1(f)} + \overline{Q_2(f)}|}{n_1 e_1^3 + n_2 e_2^3}. \tag{18}$$

The value of $|\overline{Q_1(f)}|$ is given using the velocity V_1 and the inlet section s of the n_1 fractures of thickness e_1 by:

$$|\overline{Q_1(f)}| = |V_1| \cdot n_1 \cdot s.$$

The value of $|\overline{Q_1(f)}| + |\overline{Q_2(f)}|$ which is the total quantity of flow can be estimated knowing the instantaneous velocity of the piston V_{piston} and its cross-section S_{piston}.

$$|\overline{Q_1}(f)| + |\overline{Q_2}(f)| = V_{\text{piston}} \cdot S_{\text{piston}}$$
$$= 1{,}571 \cdot 10^{-5} f \cos \omega t.$$

Thus the two last members of (18) lead to:

$$V_1 = \frac{2{,}857 \cdot 10^{-4}}{n_1 e_1^3 + n_2 e_2^3} \cdot e_1^2 \cdot f. \tag{S. I.}$$

For $R_e = 2300$; $\nu = 10^{-6}$ SI, we obtain:

$$f_c = 4.025 \cdot \frac{n_1 e_1^3 + n_2 e_2^3}{e_1^3}.$$

The field of frequency in which the theoretical linear model remains valid can therefore be approached for the 5 tests carried out

— Test 1: (two 2 mm fractures)
$f_{\text{crit.}} = 8.0$ Hz

— Test 2: (one 2 mm fracture and one 1 mm fracture)
$f_{\text{crit.}} = 4.5$ Hz

[1] To estimate the dephasing between V_1 and V_2, the complex relation (8) $\frac{1}{\bar{F}} = \frac{1}{\bar{F}_1} + \frac{1}{\bar{F}_2}$ can be used.

— Test 3: (one 4 mm fracture and one 1 mm fracture)
$f_{crit.} = 4.0$ Hz

— Test 4: (one 4 mm fracture and two 1 mm fractures)
$f_{crit.} = 5.0$ Hz

— Test 5: (one 4 mm fracture and two 2 mm fractures)
$f_{crit.} = 4.1$ Hz

But it is important to specify that this critical frequency f_c does depend on the total quantity of flow injected in the fissure, i. e. on the volume injected by the piston. *Reducing this volume makes it possible to adopt a limiting value f_c, as high as required* for the identification of the parameters.

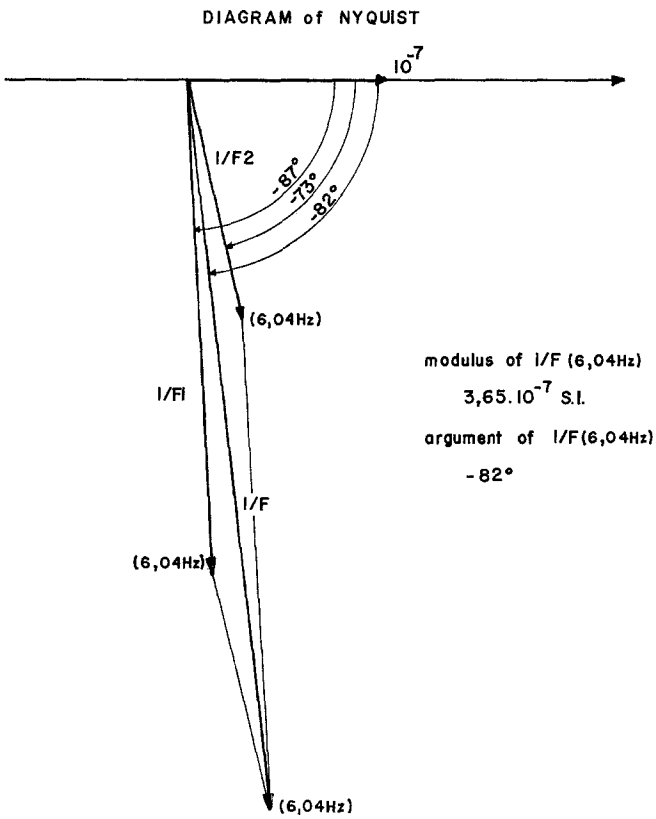

Fig. 19. Diagram of Nyquist

In the case of test No. 4, for a frequency of 6 Hz, a relative error of 3% is obtained assuming that flows $\overline{Q_1}$ and $\overline{Q_2}$ were perfectly in phase (Fig. 19)

$$\text{Relative error} = \frac{|\overline{Q_1}| + |\overline{Q_2}| - |\overline{Q_1} + \overline{Q_2}|}{|\overline{Q_2} + \overline{Q_2}|} < 3\%.$$

6. Conclusions

The purpose of this study was to extend harmonic techniques to the reconnaissance of fractured media with several sets of fractures, the case of one set of fractures having been examined by Fras et al. (1981).

The transfer function, valid for m families of fractures, with n_i fractures and opening e_i, is given in the case of inertia-viscosity models (direct problem).

The parameter identification is treated in the case of 2 families, leading to a unique determination of the mathematical parameters and the physical parameters (unicity of the inverse problem). This identification is described with knowledge of modulus and phase or modulus alone.

The case of more than two families of fractures has also been approached. In this case, the direct problem does not present any difficulty whatever the number of families may be. As far as the inverse problem is concerned, the case of three families has been examined by Portalès (1981) and the uniqueness has been proved using the two asymptotical conditions, $f \to 0$ and $f \to \infty$, and one point of the transfer function. The inverse problem could be theoretically generalized to any number of families, but in practice a limitation would probably be imposed by the accuracy of experimental data.

The comparison between theory and laboratory tests shows an excellent fit in the medium range of frequencies, giving a good verification of the direct problem modelling.

As far as the inverse problem is concerned attention should be paid in practice to measuring apparatus in order to obtain a frequency bandwidth as wide as required by the identification inverse problem, and in order to avoid problems connected with the appearance of turbulence phenomena at high frequencies.

References

Crosnier, B. (1983): Recherche de l'unicité de la solution entre paramètres mathématiques et paramètres physiques. Reconnaissance harmonique appliquée au cas de la géotechnique. Note interne de Recherche, no. 212. Laboratoire de Génie Civil, U. S. T. L. Montpellier, Mars.

Crosnier, B., Duruisseaud, P., Fras, F., Jouanna, P., Portales, J.-L. (1979): Brevet d'invention: Procédé et dispositif de reconnaissance de sols et de milieux rocheux. no. 79. 25285 — Anvar, Octobre.

Crosnier, B., Jouanna, P., Portales, J.-L. (1981): Reconnaissance de fissuration par analyse harmonique. Contrat D. G. R. S. T. no. 79. 7. 368. Géologie et Aménagement, thème Hydrogéologie en milieu fissuré. Décembre.

Fras, G. (1979): Reconnaissance de certains milieux fissurés et théorie des systèmes. Thèse de Doct. Ing., Institut National Polytechnique de Toulouse, Oct.

Fras, G., Pons, J.-C., Jouanna, P. (1981): Reconnaissance d'un système fissuré par pompage harmonique. J. Méc. Appl. 5, no. 4.

Gringarten, A. C. (1971): Unsteady-state Pressure Distribution Created by a Well with a Single Horizontal Fracture, Partial Penetration or Redistricted Entry. Ph. D. Stanford University.

Gringarten, A. C., Witherspoon, P. A. (1972): A Method of Analysing Pumptest Data from Fractured Aquifers. Compte rendu à la Conférence: "Percolation Through Fissured Rocks". Société Internationale de Mécanique des Roches, Stuttgart, Septembre.

Louis, C. (1976): Introduction à l'hydraulique des roches. Thèse d'état, Université Paris VI, Avril.

Portales, J. L. (1981): Sondes pour reconnaissance de milieux fissurés par essais harmoniques: conception des sondes, essais et interprétation. Thèse de Doct. Ing., Institut National des Sciences Appliquées de Toulouse, Septembre.

Wang, J. S. Y., Narasimhan, T. N., Tsang, C. F., Witherspoon, P. A. (1978): Transient Flow in Tight Fractures, The Invitational Well Testing Symposium, Rep. No. LSC 7027, Lawrence Berkeley Laboratory, Berkeley, May.